Tellus A
Dynamic Meteorology and Oceanography

A Case Study on Phytoplankton Blooms Triggered by Tropical Cyclone Emeraude in the Central Indian Ocean

ORIGINAL RESEARCH PAPER

YAOYAO ZHOU
HAIBIN LÜ
HAOJIE HUANG
LINFEI BAI
XIAOQI DING
ZHANGJUN CHEN

*Author affiliations can be found in the back matter of this article

STOCKHOLM UNIVERSITY PRESS

CORRESPONDING AUTHOR:
Haibin LÜ

Jiangsu Key Laboratory of Marine Bioresources and Environment/Jiangsu Key Laboratory of Marine Biotechnology, Jiangsu Ocean University, Lianyungang, Jiangsu province, China; Co-Innovation Center of Jiangsu Marine Bio-industry Technology, Jiangsu Ocean University, Lianyungang, Jiangsu province, China; School of Marine Technology and Geomatics, Jiangsu Ocean University, Lianyungang, Jiangsu province, China

haibin_lv@jou.edu.cn

ABSTRACT

Phytoplankton blooms occurred in the Central Indian Ocean after tropical cyclone (TC) Emeraude with an elliptic track in March 2016. Here, the ecological responses of the upper ocean layer were first researched based on remote sensing, reanalysis data and Argo data. The results show that two clockwise cyclonic eddies with a vorticity of 0.22 s^{-1} appeared on the southern equatorial current after the TC. Chlorophyll-a (Chl-a) blooms were found in the two eddies after the TC. The Chl-a concentration in the center of the cyclonic eddies reached 0.5 $mg{\cdot}m^{-3}$. The deepened mixed layer, weakened thermocline, and thinned barrier layer facilitated the uplift of nutrients from the deep sea to the upper layer. Additionally, the sufficient photosynthetically available radiation (PAR) over the two eddies reached 50 Einstein $m^{-2}{\cdot}day^{-1}$ after March 24, thereby providing favorable conditions for the Chl-a blooms that occurred on March 26 in Box A and March 28 in Box B. This study contributes to assessments of the ecological impacts of ocean eddies in the Central Indian Ocean after TCs.

KEYWORDS:
Chl-a; cyclonic eddies; upwelling; tropical cyclone

TO CITE THIS ARTICLE:
Zhou, Y, LÜ, H, Huang, H, Bai, L, Ding, X, Chen, Z. 2024. A Case Study on Phytoplankton Blooms Triggered by Tropical Cyclone Emeraude in the Central Indian Ocean. *Tellus A: Dynamic Meteorology and Oceanography*, 76(1): 101–114. DOI: https://doi.org/10.16993/tellusa.3242

1 INTRODUCTION

Tropical cyclones (TCs) are extreme weather events that have significant impacts on physical and biogeochemical processes in the upper ocean (Guan et al., 2019; Qiu et al., 2021; Qiu et al., 2020; Sun et al., 2021). Preexisting atmospheric disturbances, warm sea surface temperatures (SSTs) above 27°C, prevalent atmospheric instability, and lower vertical wind shear are all necessary for the formation of a TC (Kuttippurath et al., 2021).

Many scholars have conducted large-scale numerical studies on the effects of TCs on the ocean (Subrahmanyam et al., 2002). He et al. (2017) demonstrated based on a 1-D physical-biogeo chemical model that eddy-Ekman pumping was essential because it not only transported additional nutrients into the mixed layer but also led to significant chlorophyll enrichment in subsurface water (Han, Ma & Chen, 2012). TCs had a significant effect on the rise in primary production in the ocean (Lin et al., 2003). A series of chemical and biological dynamics in the surface water can be triggered by the pumping of inorganic nutrients from deep water to the surface (Chen et al., 2006). Additionly, phytoplankton blooms are also heavily influenced by an increase in the nitrate concentration (Lin et al., 2009). Kubryakov, Zatsepin and Stanichny (2019) concluded that chlorophyll bursts may be caused by the interactions among four physical factors: turbulent entrainment caused by wind, diapycnal mixing due to inertial current vertical shear, basin-scale Ekman pumping, and local Ekman upwelling. Some studies have shown earthquakes and volcanic eruption may change the SST and increase the upwelling of eutrophic water (Jing et al., 2020; Singh et al., 2006). Kundu et al. (2010) discussed the phenomenon of pronounced change in the chlorophyll concentrations after the super cyclone Orissa. Offshore blooms may also be triggered by upwelling and entrainment induced by strong typhoons and the topography of islands and islets (Zhao, Tang & Wang, 2009).

Dey and Singh (2003) used IRS-P4 Ocean Color Monitor data to compare chlorophyll concentrations in the northeastern Arabian Sea and the southern Bay of Bengal. Many scholars have found that coupling between the land-ocean-atmosphere associated with TCs occurred in this region (Chauhan, Kumar & Singh, 2018; Chauhan et al., 2021). Stratification and mixing are produced in the upper ocean due to atmospheric forcing, which can cause surface phytoplankton blooms lasting from days to weeks (Carranza & Gille, 2015). At various scales, all of these physical forcings have the potential to decrease the water-column stability and increase vertical mixing (Chu et al., 2000). Ekman pumping can be significantly influenced by the atmospheric cyclonic wind stress curl, resulting in upwelling beneath a typhoon's center (Wang et al., 2020; Zhou, Tian & Wang, 2005). Vertical mixing caused by wind can deepen the mixed layer and carry nutrients and chlorophyll-a (Chl-a) to the sea surface from the subsurface layers (Kubryakov, Zatsepin & Stanichny, 2019; Vinayachandran, 2003). During the process of TCs, the land meteorological and atmospheric parameters can also change dramatically (Chauhan et al., 2020; Tang et al., 2009). Furthermore, near-inertial internal waves have also been observed during and after TC passage, and these waves exert force and torque on cylindrical tendon legs (LÜ et al., 2016).

Although the response of the ocean to TCs has been the subject of extensive research, few studies on TCs have been carried out over the southern equatorial current in the central Indian Ocean. The rarity of TC Emeraude provides a unique opportunity to investigate the upper ocean's response in the central Indian Ocean.

In this manuscript, we have carried out detailed analysis of ocean parameters after TC Emeraude using remote sensing, reanalysis data, Argo data and the results show the pronounced ecological responses of the upper ocean.

2 DATA AND METHODS

2.1 STUDY AREA

The study area's geographical location and the TC trajectory are depicted in Figure 1. Two boxes are selected on the clockwise cyclonic eddies in the study area, namely, Box A (9°S–12°S, 82°E–85°E) and Box B (9.5°S–12.5°S, 85.2°E–88.2°E). TC Emeraude originated from 86.8°E, 11.3°S on March 15, 2016, in the central Indian Ocean and eventually disappeared near its starting location on March 21, 2016.

2.2 DATA

We analyzed various oceanic and meteorological parameters using reanalysis data, Argo data and satellite remote sensing data. The relevant details are as follows.

The Joint Typhoon Warning Center (JTWC) (https://www.metoc.navy.mil/jtwc/jtwc.html) provided the basic TC track data; this center provides cyclone forecasts for the Southern Ocean. The data contain the maximum persistence of the tropical cyclone recorded every 6 hours, near-ground winds and the center of the tropical cyclone.

The Global Marine Copernicus Marine Environmental Monitoring Service (CMEMS) (http://marine.copernicus.eu/) collected salinity, temperature, current eddy, SSH, surface wind, global mixed mean wind field (including wind stress, wind stress curl, and meridional and latitudinal wind components), dissolved iron, and nutrient information (Tan et al., 2022).

The climatology nitrate concentration in March was obtained from the World Ocean Atlas 2018 (WOA18,

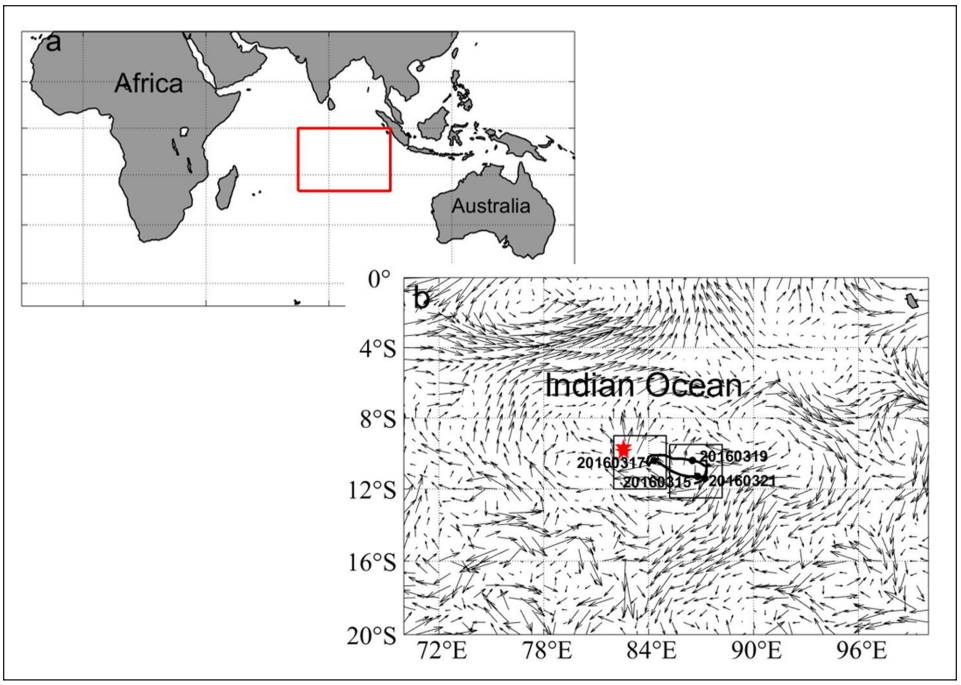

Figure 1 The study area's geographical location and the TC trajectory with the flow field (black arrow). The Argo buoy is marked by the star (number 1901447). Box A: 9°S-12°S, 82°E-85°E; Box B: 9.5°S-12.5°S, 85.2°E-88.2°E.

https://www.nodc.noaa.gov/OC5/woa18/woa18data.html) at a 1° × 1° resolution.

The daily Chl-a concentrations and photosynthetically available radiation (PAR) data were both obtained from the GlobColor project, which provides continuous L3 marine color remote sensing data products at a spatial resolution of 4 km × 4 km. The website from which the data were obtained is as follows: http://hermes.acri.fr/index.php?class=archive.

The daily sea surface wind field vector data were sourced from the Cross-Calibrated Multi-Platform (CCMP, http://www.remss.com/measurements/ccmp) at a spatial resolution of 0.25° × 0.25°. The L3 wind field analysis dataset has a spatial and temporal resolution suitable for scientific research. These wind field data were used in this study to calculate the Ekman suction velocity.

The vertical profile data representing temperature and salinity were provided by the Argo program (http://www.argodatamgt.org/). Platform number 1901447 was selected for use in this paper; this platform not only provides real-time temperature and salinity observations throughout the lifetime of the TC at different depths from 1 March to 31 March 2016 but was also used here to calculate the buoyancy frequency.

2.3 METHODS

In this paper, the Ekman pumping velocity and vertical vorticity are calculated for the vertical effect of the TC. Furthermore, the buoyancy frequency, turbulent mixing rate, mixing layer depth, and isotherm depth using Argo data are proposed to study the ocean stratification.

2.3.1 Ekman pumping velocity (EPV)

Since the wind stress and Coriolis parameter on the surface of the ocean change spatially, convergence and divergence occur in the horizontal direction. An estimate of the study area's surface Ekman pumping velocity was made for a mechanistic exploration of the chlorophyll burst. The velocity was calculated as follows (Kubryakov, Zatsepin & Stanichny, 2019):

$$W_E = \nabla \times \tau / \rho f \quad (1)$$

where ρ represents the density of water, τ is the wind stress, and f is the Coriolis parameter.

2.3.2 Buoyancy frequency

After a stable stratification is disturbed, fluid particles move vertically and oscillate due to inertia and the combined action of gravity and buoyancy. The buoyancy frequency of these oscillations can be calculated as follows:

$$N^2 = -g\rho^{-1} d\rho / dz \quad (2)$$

where g is the acceleration of gravity, ρ is the density of water, and $d(\rho)/d(z)$ represents the derivative of the potential density with respect to the vertical coordinate z.

2.3.3 Turbulence mixing rate

As TCs affect the upper ocean, very strong vertical mixing occurs in the ocean, and the turbulent mixing rate in this turbulent motion can be calculated through the turbulent kinetic energy dissipation rate; here, he turbulent mixing rate K_ρ was determined (MacKinnon & Gregg, 2003) as follows:

$$K_\rho = \Gamma \varepsilon / N^2 \quad (3)$$

where Γ is the efficiency coefficient of the mixture, with a recommended value is 0.2 according to the Osborn study (Osborn, 1980), ε is the rate of turbulence dissipation and N is the buoyancy frequency.

2.3.4 Vertical vorticity

The following current vector's curl (u, v) is used to describe the generation and disappearance of eddies before and after the passage of TC Emeraude (Lü et al., 2021):

$$\text{curl} = dv/dx - du/dy \quad (4)$$

where the x and y components of the velocity are represented by u and v, respectively.

2.3.5 Mixed layer depth (MLD) and isothermal layer depth (ILD)

The MLD is a uniform-density and uniform-temperature layer that serves as the air-sea interface (Balaguru et al., 2012). The MLD is defined as an increase in the relative potential density to the surface ($\Delta\sigma_\theta$) when the SST decreases by (T = −0.5 °C) equal to the depth of the increased surface potential density (D) (de Boyer Montégut, 2004):

$$\Delta\sigma_\theta = \sigma_{MLD} - \sigma_{10}, \quad (5)$$

$$\Delta\sigma_\theta = \sigma_\theta(T_{10} + \Delta T, S_{10}, P_0) - \sigma_\theta(T_{10}, S_{10}, P_0), \quad (6)$$

$$MLD = D(\sigma_{MLD}), \quad (7)$$

where P_0 is the pressure at the ocean's surface and the salinity and temperature values at the reference surface (10 m) are referred to as T_{10} and S_{10}. ILD is defined as the depth (D) at which the temperature is 0.5 °C below the surface (10 m).

$$\Delta T = T_{ILD} - T_{10}, \quad (8)$$

$$ILD = D(T_{ILD}), \quad (9)$$

3 RESULTS

We present a detailed analysis of ocean parameters obtained from reanalyzed data, such as climatology nitrate,sea surface current and SST, PAR, which can play an important role in the ecological response of the TC. Detailed analysis is proposed for the phytoplankton blooms in the study area.

3.1 CLIMATOLOGY NITRATE

Nutrients in seawater are the material basis for phytoplankton blooms. According to the climatology

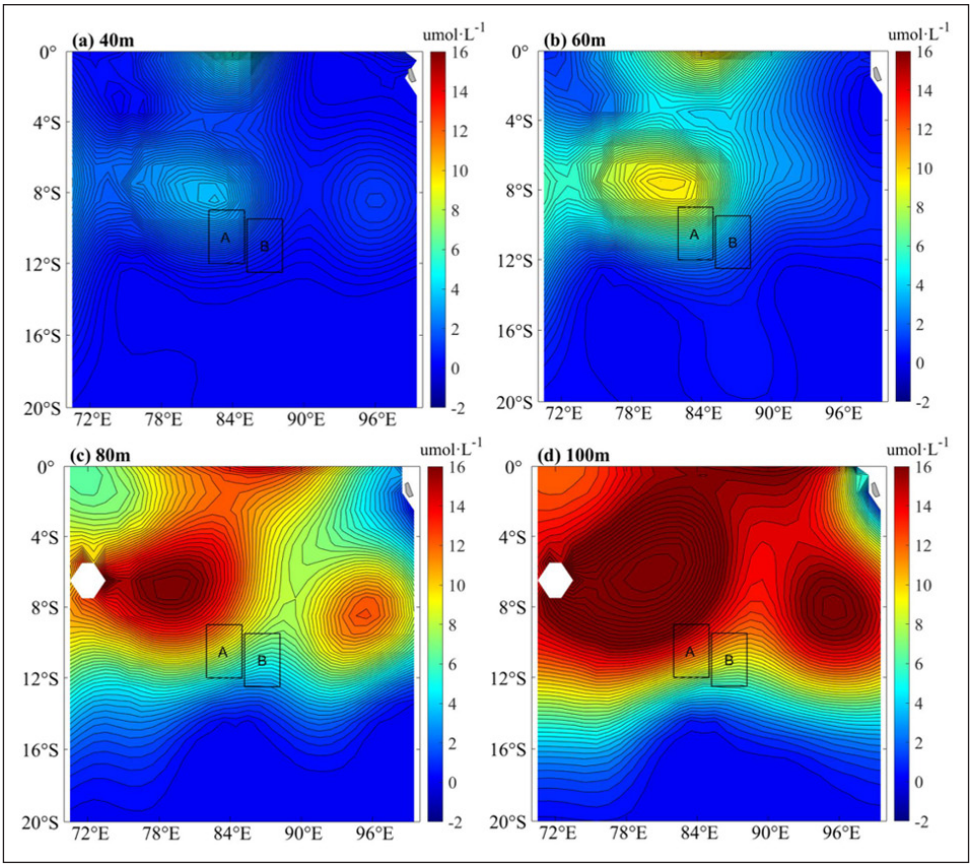

Figure 2 Climatology nitrate concentrations (μmol·L⁻¹) at different depths in March 2016 (**a, b, c**, and **d** denote the nitrate concentrations at depths of 40 m, 60 m, 80 m, and 100 m, respectively).

nitrate data in March, as shown in Figure 2, the nitrate concentrations were found to range from z = 40 m to 60 m, 80 m, and 100 m. The high-nitrate-concentration region was distributed at two clockwise cyclonic eddies. The nitrate concentration reached 2 μmol·L^{-1} (16 μmol·L^{-1}) at a depth of 40 m (100 m) (Figure 2). We found that submarine nitrate rose with upwelling, thereby contributing to Chl-a blooms in the upper ocean.

3.2 PATH OF TC AND WIND FIELD

Depending on the near-center maximum wind speed (MWS), TCs can be categorized as follows: deep depression (13.7–17.0 m·s^{-1}), cyclonic storm (17.0–25.0 m·s^{-1}), severe cyclonic storm (25.0–32.5 m·s^{-1}), very severe cyclonic storm (32.5–46.0 m·s^{-1}), extremely severe cyclonic storm (46.0–61.1 m·s^{-1}), and super cyclonic storm (≥61.1 m·s^{-1}).

Table 1 illustrates the studied TC's MSW position, time, and location. TC Emeraude originated from 86.8°E, 11.3°S on March 15, 2016, in the Central Indian Ocean and disappeared on March 21, 2016, at 86.6°E, 11.7°S. At 12:00 on March 17, TC Emeraude strengthened to an extremely severe cyclonic storm with a maximum wind speed of 57.5 m·s^{-1}; then, the speed promptly decreased to a severe cyclonic storm. At 12:00 on March 19, the brief enhancement was reduced to a very severe cyclonic storm with a maximum wind speed of 37.5 m·s^{-1} before finally decreasing to a cyclonic storm and deep depression.

LAT (°S)	LON (°E)	TIME	MSW (M/S)
11.3	86.8	03/15/06	12.5
11.3	86.3	03/15/12	15
11.0	85.3	03/16/00	27.5
10.6	84.7	03/16/12	37.5
10.4	84.3	03/17/00	50.5
10.7	84.0	03/17/12	57.5
10.1	84.2	03/18/00	45
10.3	85.4	03/18/12	32.5
10.4	86.5	03/19/00	32.5
10.7	87.2	03/19/12	37.5
10.7	87.5	03/20/00	32.5
10.8	87.3	03/20/12	25
11.4	87.2	03/21/00	20
11.7	86.6	03/21/12	12.5

Table 1 Position, time, and MSW (maximum wind speed) of the studied TC.

3.3 SEA SURFACE CURRENT AND SST

The sea surface currents and SSTs at different times during the development of the TC are shown in Figure 3 during the TC passage, two weaker cyclonic eddies appeared in the study area. The intensity of these two cyclonic eddies increased, and they continued for more than one month after the TC.

In response to TCs, SST cooling is a major oceanic phenomenon that can be influenced by the strength of the TC and the wind speed. Figure 4 shows the spatially averaged time series of SSTs from March 1 to March 31. Generally, TCs cool the ocean surface by several degrees along their track (Neetu et al., 2012). Roughly the same decrease in SSTs was observed in the two boxes from March 15 to March 21. The maximum temperature difference reached approximately 2°C.

3.3 CHL-A

Figure 5 shows the locations of Chl-a on March 23, March 24, March 27, and March 28, 2016. The strong cyclonic eddy in Box A occurred earlier than that in Box B, and the same characteristics were found for the Chl-a blooms. A Chl-a bloom occurred in Box B with a maximum concentration of 0.5 mg·m^{-3}, significantly higher than that in Box A. Figure 6 shows the spatially averaged Chl-a concentrations from March 1 to March 31 in Boxes A and B.The Chl-a did not change too much during non-cyclonic periods, less than 0.02 mg·m^{-3}. Five days after the TC had passed, the Chl-a concentrations in Boxes A and B reached their maximum values of 0.03 mg·m^{-3} and 0.087 mg·m^{-3} on March 27 and March 28, respectively.

Table 2 counts the name, position and time of the TC in 2011–2019 in this region.The phenomenon of a Chl-a eruption occurred after the TC CHERONO in 2011. By comparison, we found that the TC Emeraude developed clockwise, forming an elliptic track.The Chl-a blooms were found in the two clockwise cyclonic eddies associated with the TC. This is different and interesting from the other years.

3.5 PHOTOSYNTHETICALLY AVAILABLE RADIATION (PAR)

PAR has an important impact on Chl-a blooms. The passage of a TC may cause upwelling and ocean mixing (Subrahmanyam et al., 2002), bringing submarine nutrient-rich water up to the euphotic zone, which is rich in light for photosynthesis but often lacks nutrients. Figure 7 shows the changes in the spatially averaged PAR over time in Boxes A and B. During the passage of the TC, the PAR in Box A fell on March 15, while the spatially averaged PAR in Box B dropped from March 13 to March 20. On March 24, the PAR in the two boxes reached 50 Einstein m^{-2} day^{-1} and attained a steady state, Thus providing favorable conditions for the Chl-a blooms that occurred on March 26 in Box A and March 28 in Box B.

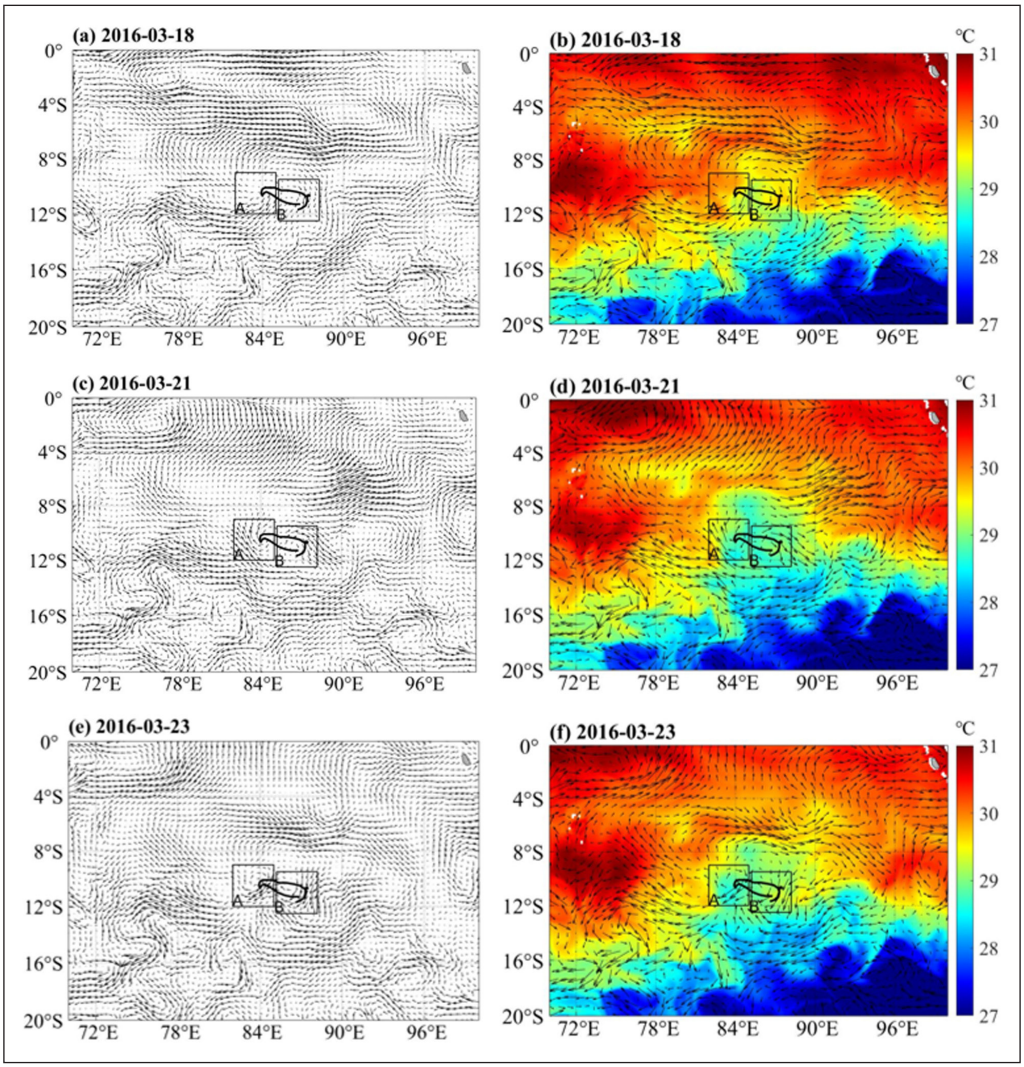

Figure 3 Sea surface currents (in units of m·s^{-1}) and SSTs during the development of the TC. Panels **(a)**, **(c)**, and **(e)** showthe changes in the flow field (arrows) on March 18, March 21, and March 23, 2016, respectively; panels **(b)**, **(d)**, and **(f)** show the SST changes on March 18, March 21, and March 23, 2016, respectively, and the color bar represents the SST (°C).

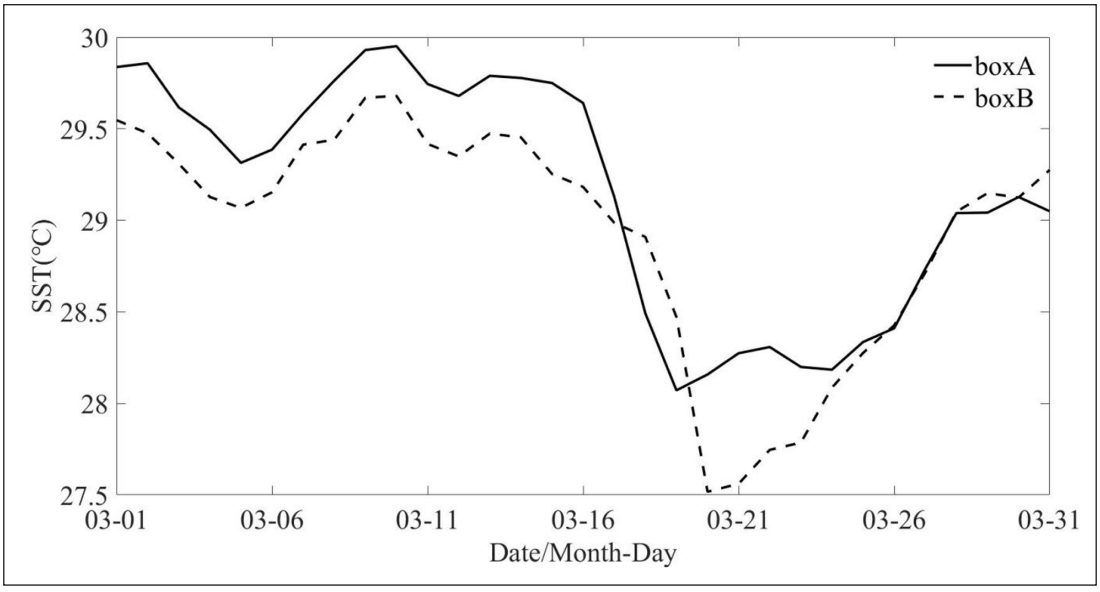

Figure 4 Spatially averaged SSTs from March 1 to March 31 in Boxes A and B.

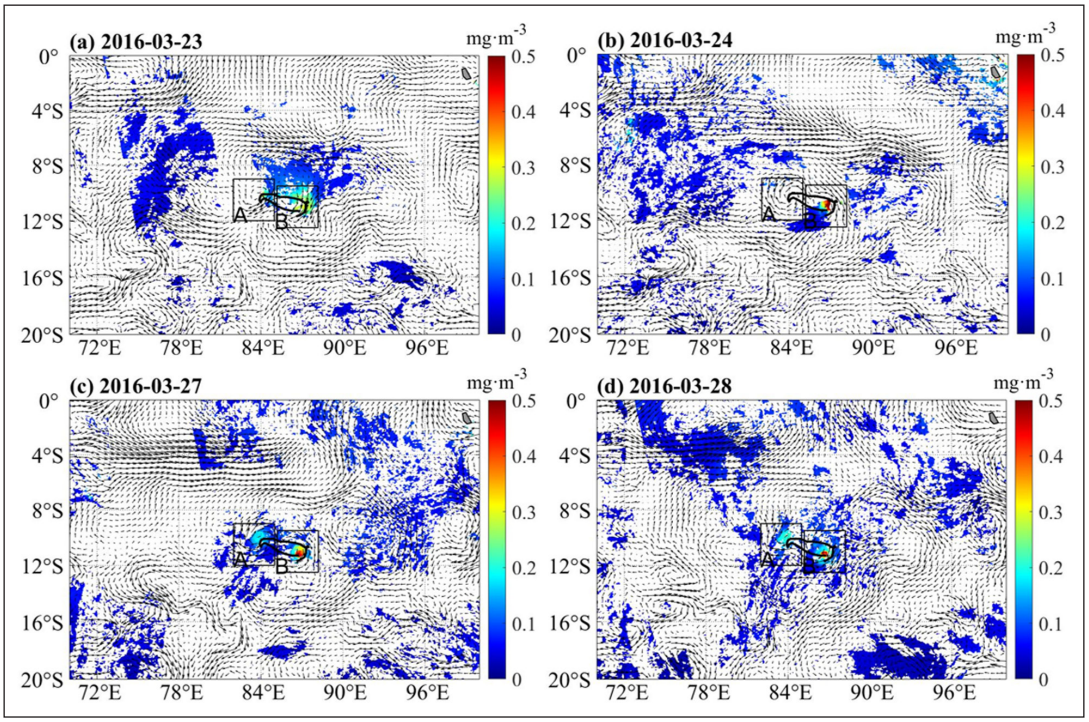

Figure 5 Concentrations of Chl-a and surface flows (black arrow) at diverse times. Panels **(a)**, **(b)**, **(c)**, and **(d)** show the changes in Chl-a on March 23, March 24, March 27, and March 28, 2016, respectively.

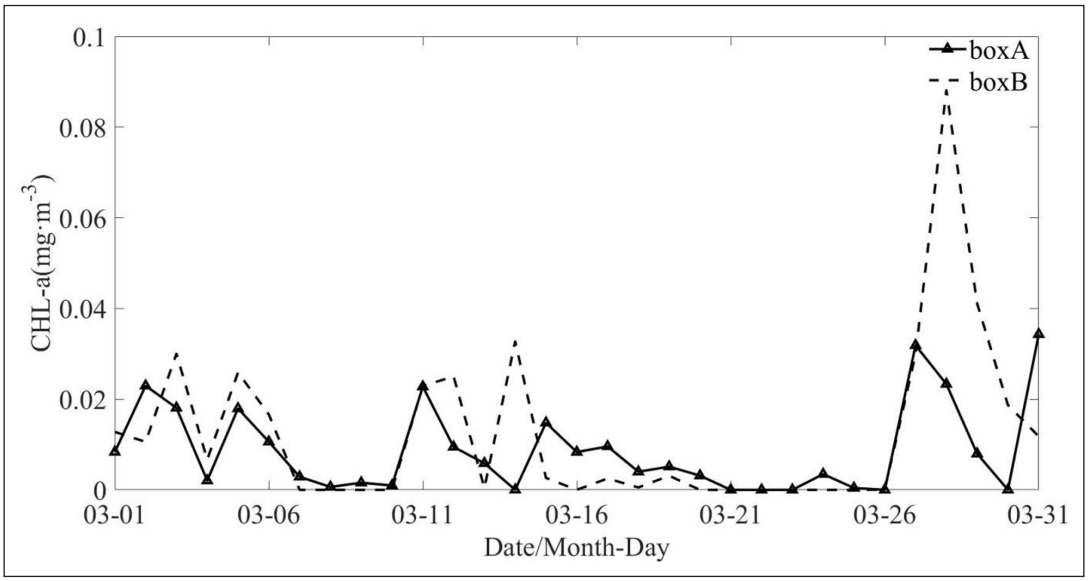

Figure 6 Spatially averaged chl-a concentrations from March 1 to March 31 in Boxes A and B.

YEARS	TC NAME	TIME	LAT RANGE (°S)	LON RANGE(°E)	PHYTOPLANKTON BLOOMS
2011	CHERONO	03/14–03/23	11.3–27.5	57–87.7	Yes
2013	JAMALA	05/07–05/15	5.8–10.7	80.2–88.7	No
2015	IKOLA	04/04–04/08	10.5–22	86.6–99	No
2019	LORNA	04/21–04/30	4–23.9	79.3–90	No

Table 2 Position, time of the TC in 2011–2019.

4 DISCUSSION

4.1 ROLES OF TCs

Ekman transport and Ekman pumping are known to promote coastal upwelling (Zhao, Tang & Wang, 2009). The EPV triggered by TCs can be calculated using (1) in Section 2. Figure 8 depicts the EPV during the passage of the studied TC. The upwelling in Box A increased significantly on March 17 and March 18. Box B showed clear enhanced upwelling on March 19 and March 20. The velocities of these two boxes both reached 2 × 10^{-4} m s^{-1}. TC-induced upwelling may uptake nutrients to the upper ocean, thereby contributing to Chl-a blooms.

Figure 9 shows the water temperatures at various depths in Boxes A and B. After the TC, cold submarine water rose with vertical mixing, entrainment, and upwelling. TCs can reconstruct stratification and bring abundant nutrients to the upper ocean, positively affecting phytoplankton growth. Thus, the concentration of phytoplankton Chl-a also increases (Zhao et al., 2015). SST cooling has even been used as a proxy for phytoplankton blooms (Sarangi, Mishra & Chauhan, 2015).

4.2 ROLES OF STRATIFICATION

Figure 10 shows the vertical distribution of the buoyancy frequency before and after TC passage. The mixed layer

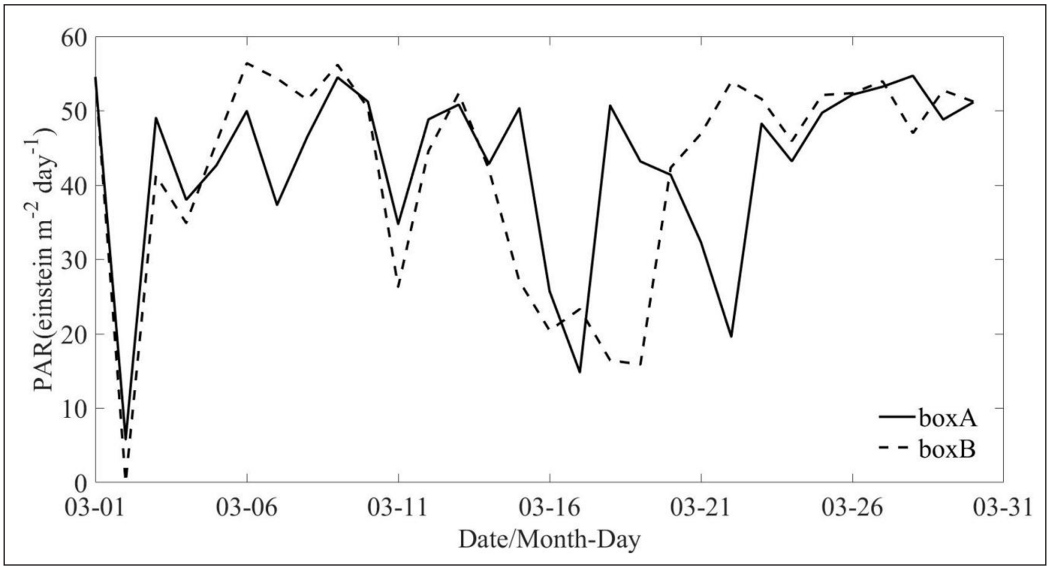

Figure 7 Spatially averaged PAR from March 1 to March 31 in Boxes A and B.

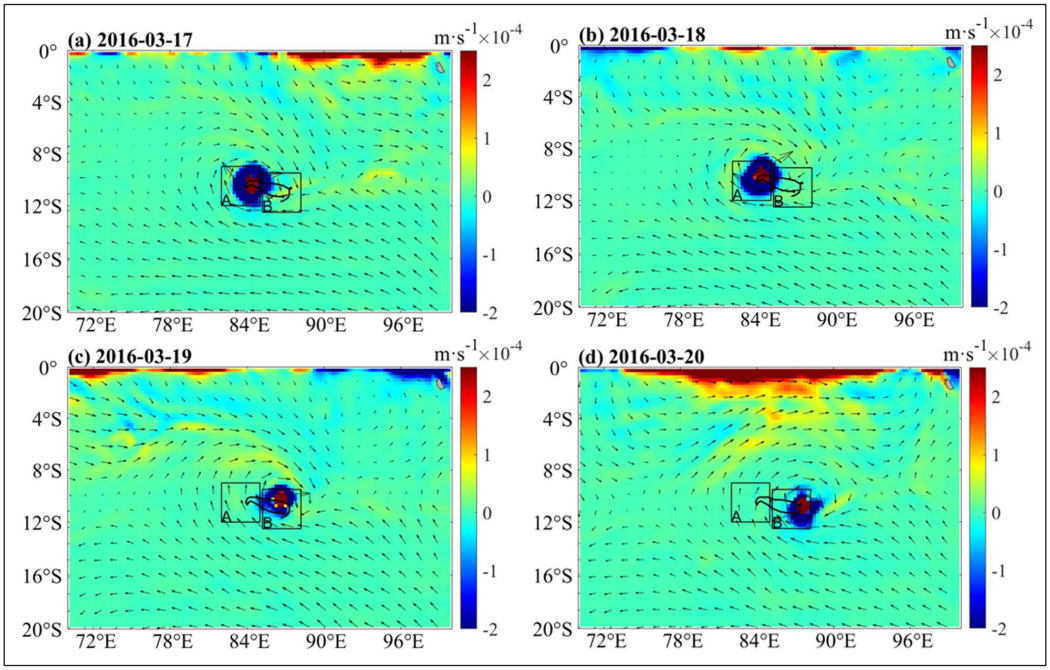

Figure 8 Surface wind speeds (black arrow) and EPVs during the passage of the studied TC (unit: m/s).

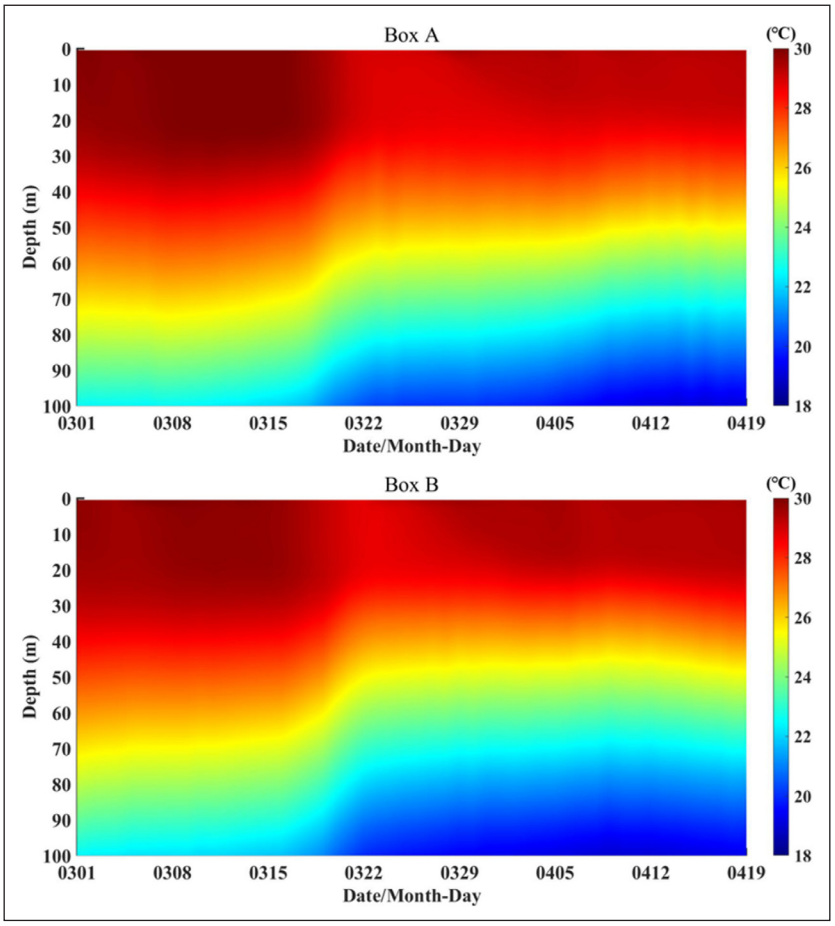

Figure 9 Time series of temperatures at various depths in Boxes A and B.

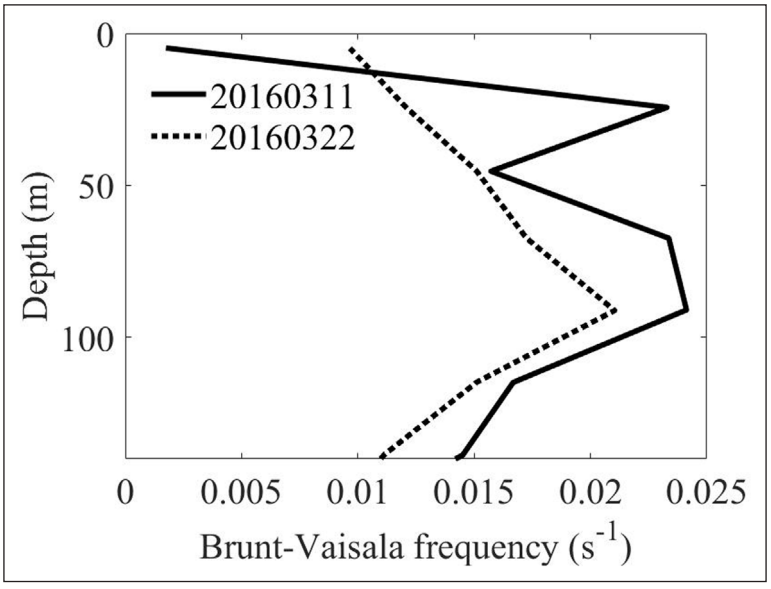

Figure 10 Vertical distribution of the buoyancy frequency before and after the TC.

depth and isothermal layer depth from Argo floats on March 11 and March 22 are shown in Figure 11 in the Indian Ocean, due to the effect of salinity on near-surface stratification, there is an additional interlayer between the base of the mixed layer and the top of the thermocline, namely, the barrier layer (Sprintall & Tomczak, 1992). Before and after the TC passage, the MLD changed from 13.7 m on March 11 to 27.5 m on March 22. The ILD changed from 27.5 m on March 11 to 34.5 m on March 22. The maximum buoyancy frequency (N) changed from 0.024 s^{-1} to 0.021 s^{-1}. The thickness of the barrier layer changed from 13.8 m to 7 m. Obviously, a deepened mixed layer, weakened thermocline, and thinned barrier layer can facilitate the uplift of nutrients

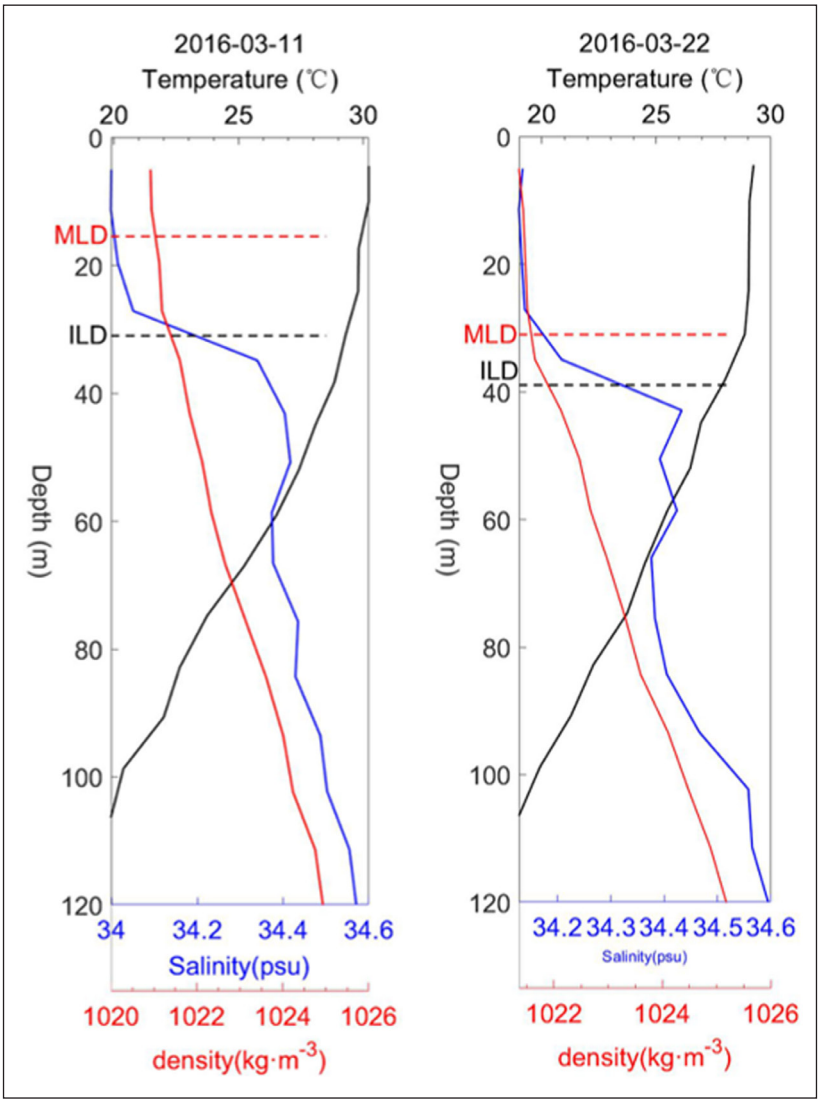

Figure 11 MLD and ILD data from Argo floats on March 11 and March 22.

from the deep sea to the upper layer (Wang et al., 2022). A similar phenomenon also occurred near the Luzon Strait, where the MLD deepened from 20 m to 56 m with a decrease in the temperature after Typhoon Parma, and a Chl-a bloom occurred, likely due to the upwelling of nutrients (Zhao et al., 2013).

4.3 VERTICAL MIXING

Enhanced turbulent mixing in the upper ocean helps transport nutrient-rich cold water from the lower layer to the light-permeable layer; this is the main mechanism by which low-temperature phytoplankton blooms are maintained in this region (Wang et al., 2020). When a TC affects the upper ocean, very strong vertical mixing occurs in the upper ocean, causing sea cooling in the mixed layer. According to Figure 11, the mixed layer is significantly deepened. Figure 12 shows the daily average turbulent eddy diffusivity on March 11 and March 22. Affected by the TC Emeraude, the average mixing rate increased. The mixing rate roughly decreased with increasing depths, and the mixing rate of the upper mixing layer was significantly greater than that of the bottom layer. The maximum $K\rho$ value on March 11 (March 22) was 2.50×10^{-4} $m^2 \cdot s^{-1}$ (3.54×10^{-4} $m^2 \cdot s^{-1}$) in the upper ocean.

Figure 13 shows the time series of vorticities at diverse depths in Boxes A and B. After the TC passage, the intensity of both cyclonic eddies increased and persisted for a long time with a maximum vorticity of 0.22 s^{-1}. Affected by the TC, strong vertical mixing occurred on March 21. From March 27 to March 31, the vorticity above a depth of 70 m reached 0.2 s^{-1}, and the maximum vorticity value above a depth of 40 m reached 0.22 s^{-1} in Box A. Meanwhile, the maximum vorticity value reached 0.22 s^{-1} in Box B at a depth of 70 m. Therefore, it can be argued that the two reinforcing cyclonic eddies drove the deep nutrient-rich seawater up to the upper ocean by mixing and upwelling after the TC passage.

5 CONCLUSION

In this study, the response mechanism of phytoplankton blooms to TC Emeraude was analyzed by satellite

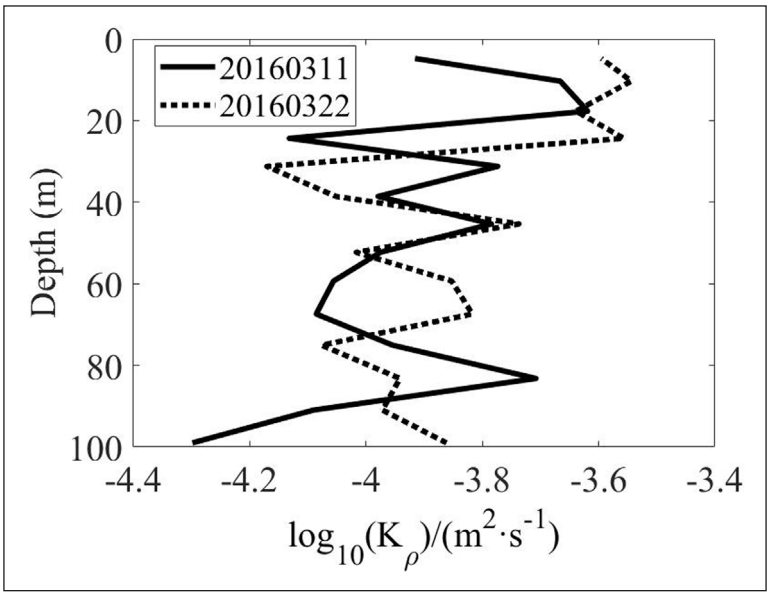

Figure 12 Daily average turbulent eddy diffusivity (Kρ).

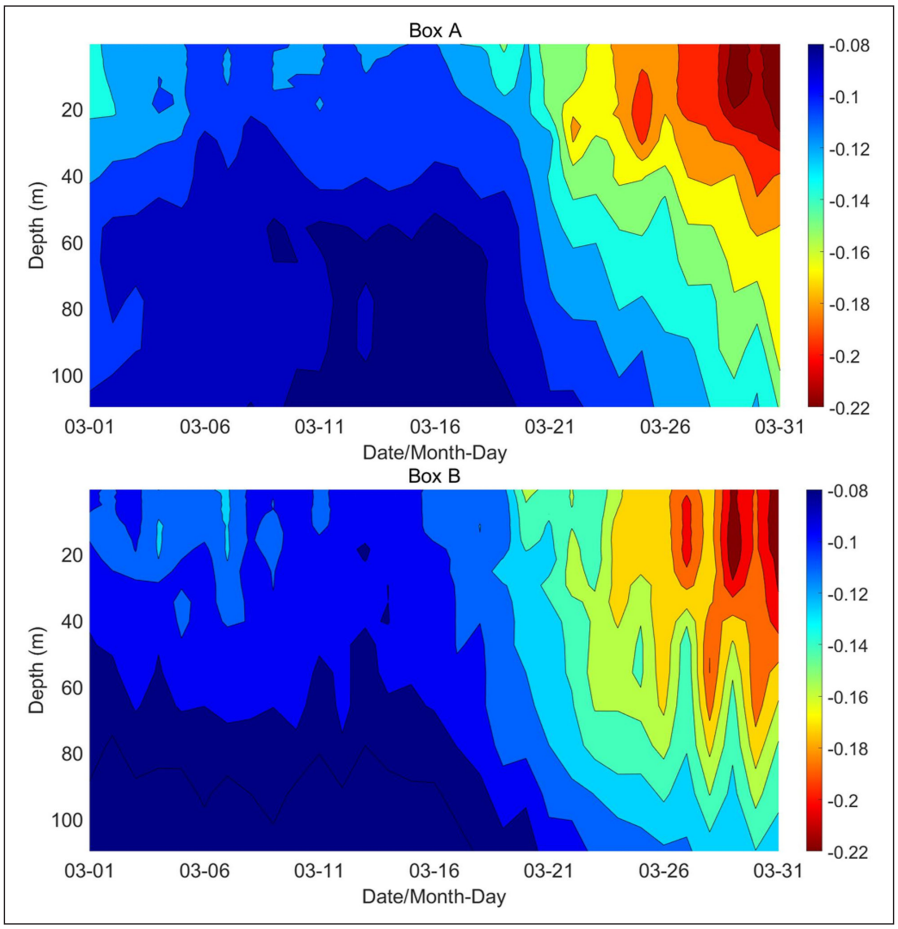

Figure 13 Time series of vorticities at diverse depths in Boxes A and B.

remote sensing, reanalysis data and Argo data during the passage of TC, and the following conclusions were drawn:

1. After the discovery of a tropical cyclone, two clockwise eddies appeared in the southern equatorial stream of the central Indian Ocean. The vorticity was also enhanced from 0.08 s^{-1} to 0.22 s^{-1}. Chl-a blooms were found in the two eddies. The chlorophyll concentration in the center of the eddies reached 0.5 $mg{\cdot}m^{-3}$.
2. Before and after the TC passage, the MLD changed from 13.7 m on March 11 to 27.5 m on March 22. The ILD changed from 27.5 m on March 11 to 34.5

m on March 22. The maximum buoyancy frequency N changed from 0.024 s^{-1} to 0.021 s^{-1}. The thickness of the barrier layer changed from 13.8 m to 7 m. Obviously, the deepened mixed layer, weakened thermocline, and thinned barrier layer facilitated the uplift of nutrients from the deep sea to the upper layer.

3. After March 24, the PAR in the two boxes reached 50 Einstein m^{-2} day^{-1} and attained a steady state, thus providing favorable conditions for the Chl-a blooms that occurred on March 26 in Box A and March 28 in Box B.

DATA ACCESSIBILITY STATEMENTS

Data can be available from Joint Typhoon Warning Center (JTWC;https://www.metoc.navy.mil/jtwc/jtwc.html), current velocity data are derived from the Copernicus Marine Environment Monitoring Service (CMEMS, (http://marine.copernicus.eu/), Nitrate distribution data from the World Ocean Atlas 2018 (WOA18, https://www.nodc.noaa.gov/OC5/woa18/woa18data.html),the Cross-Calibrated Multi-Platform (CCMP, http://www.remss.com/measurements/ccmp), with daily Chl-a and PAR data from GlobColor (http://hermes.acri. fr/index.php?class=archive). The temperature and salinity below the ocean surface are from the Indian Argo project (https://dataselection.euro-argo.eu/).

ACKNOWLEDGEMENTS

We thank the Joint Typhoon Warning Center (JTWC, https://www.metoc.navy.mil/jtwc/jtwc.html), the Copernicus Marine Environment Monitoring Service (CMEMS, (http://marine.copernicus.eu/) for current velocity,Nitrate distribution data from the World Ocean Atlas 2018 (WOA18, https://www.nodc.noaa.gov/OC5/woa18/woa18data.html), the Cross-Calibrated Multi-Platform (CCMP, http://www.remss.com/measurements/ccmp), with daily Chl-a and PAR data from GlobColor (http://hermes.acri. fr/index.php?class=archive). The temperature and salinity below the ocean surface are from the Indian Argo project (https://dataselection.euro-argo.eu/).

FUNDING INFORMATION

This work was funded by the Priority Academic Program Development of Jiangsu Higher Education Institutions (PAPD), the Postgraduate Research and Practice Innovation Program of Jiangsu Ocean University (Grants no. KYCX2022-27, KYCX2022-29, KYCX2022-70), the Postgraduate Research and Practice Innovation Program of Jiangsu Province (Grants no. SJCX22_1657) and the National Natural Science Foundation of China (Grants no. 62071207).

COMPETING INTERESTS

The authors have no competing interests to declare.

AUTHOR CONTRIBUTIONS

Conceptualization: Y.Z., X.D., H.L., H.H. and L.B.; Methodology: Y.Z., H.H., J.T., X.D. and H.L.; Validation: Y.Z., H.L., X.D. and H.L.; Formal analysis: Y.Z., Z.C., H.H., L.B. and H.H.; Investigation: Y.Z., H.L., X.D., L.B. and Z.C. ; Writing—original draft preparation: Y.Z., L.B. and H.H.; Writing—review and editing, Y.Z., H.L. and H.H.; Visualization, R.W. and X.D.; Project administration, R.W. and H.L.; Funding acquisition, Y.Z. , H.L. and Z.C.

AUTHOR AFFILIATIONS

Yaoyao Zhou
Jiangsu Key Laboratory of Marine Bioresources and Environment/Jiangsu Key Laboratory of Marine Biotechnology, Jiangsu Ocean University, Lianyungang, Jiangsu province, China; Co-Innovation Center of Jiangsu Marine Bio-industry Technology, Jiangsu Ocean University, Lianyungang, Jiangsu province, China; Lianyungang Meteorological Bureau, Lianyungang, Jiangsu province, China; School of Marine Technology and Geomatics, Jiangsu Ocean University, Lianyungang, Jiangsu province, China

Haibin LÜ orcid.org/0000-0001-8007-6619
Jiangsu Key Laboratory of Marine Bioresources and Environment/Jiangsu Key Laboratory of Marine Biotechnology, Jiangsu Ocean University, Lianyungang, Jiangsu province, China; Co-Innovation Center of Jiangsu Marine Bio-industry Technology, Jiangsu Ocean University, Lianyungang, Jiangsu province, China; School of Marine Technology and Geomatics, Jiangsu Ocean University, Lianyungang, Jiangsu province, China

Haojie Huang
School of Marine Technology and Geomatics, Jiangsu Ocean University, Lianyungang, Jiangsu province, China

Linfei Bai
Lianyungang Meteorological Bureau, Lianyungang, Jiangsu province, China; School of Marine Technology and Geomatics, Jiangsu Ocean University, Lianyungang, Jiangsu province, China

Xiaoqi Ding
Lianyungang Meteorological Bureau, Lianyungang, Jiangsu province, China; School of Marine Technology and Geomatics, Jiangsu Ocean University, Lianyungang, Jiangsu province, China

Zhangjun Chen
School of Marine Technology and Geomatics, Jiangsu Ocean University, Lianyungang, Jiangsu province, China

REFERENCES

Balaguru, K, Chang, P, Saravanan, R, Leung, LR, Xu, Z, Li, M and **Hsieh, JS.** 2012. Ocean barrier layers' effect on tropical cyclone intensification. *Proc Natl Acad Sci U S A*, 109(36): 14343–14347. DOI: https://doi.org/10.1073/pnas.1201364109

Carranza, MM and **Gille, ST.** 2015. Southern Ocean wind-driven entrainment enhances satellite chlorophyll-a through the summer. *Journal of Geophysical Research: Oceans*, 120(1): 304–323. DOI: https://doi.org/10.1002/2014JC010203

Chauhan, A, Kumar, R and **Singh, RP.** 2018. Coupling between Land(-)Ocean(-)Atmosphere and Pronounced Changes in Atmospheric/Meteorological Parameters Associated with the Hudhud Cyclone of October 2014. *Int J Environ Res Public Health*, 15(12). DOI: https://doi.org/10.3390/ijerph15122759

Chauhan, A, Singh, R, Kumar, R and **Dash, P.** 2020. Change in Land and Ocean Parameters Along the Track of Tropical Cyclone Fani of chapter. In: *IGARSS 2020 – 2020 IEEE International Geoscience and Remote Sensing Symposium*, Waikoloa, PA on 2 October 2020, pp. 5554–5557. DOI: https://doi.org/10.1109/IGARSS39084.2020.9324323

Chauhan, A, Singh, RP, Dash, P and **Kumar, R.** 2021. Impact of tropical cyclone "Fani" on land, ocean, atmospheric and meteorological parameters. *Mar Pollut Bull*, 162: 111844. DOI: https://doi.org/10.1016/j.marpolbul.2020.111844

Chen, CC, Shiah, FK, Chung, SW and **Liu, KK.** 2006. Winter phytoplankton blooms in the shallow mixed layer of the South China Sea enhanced by upwelling. *Journal of Marine Systems*, 59(1–2): 97–110. DOI: https://doi.org/10.1016/j.jmarsys.2005.09.002

Chu, PC, Veneziano, JM, Fan, C, Carron, MJ and **Liu, WT.** 2000. Response of the South China Sea to Tropical Cyclone Ernie 1996. *Journal of Geophysical Research: Oceans*, 105(C6): 13991–14009. DOI: https://doi.org/10.1029/2000JC900035

de Boyer Montégut, C. 2004. Mixed layer depth over the global ocean: An examination of profile data and a profile-based climatology. *Journal of Geophysical Research*, 109(C12). DOI: https://doi.org/10.1029/2004JC002378

Dey, S and **Singh, RP.** 2003. Comparison of chlorophyll distributions in the northeastern Arabian Sea and southern Bay of Bengal using IRS-P4 Ocean Color Monitor data. *Remote Sensing of Environment*, 85(4): 424–428. DOI: https://doi.org/10.1016/S0034-4257(03)00025-7

Guan, M, Li, Q, Zhu, J, Wang, C, Zhou, L, Huang, C and **Ding, K.** 2019. A method of establishing an instantaneous water level model for tide correction. *Ocean Engineering*, 171: 324–331. DOI: https://doi.org/10.1016/j.oceaneng.2018.11.016

Han, G, Ma, Z and **Chen, N.** 2012. Hurricane Igor impacts on the stratification and phytoplankton bloom over the Grand Banks. *Journal of Marine Systems*, 100–101: 19–25. DOI: https://doi.org/10.1016/j.jmarsys.2012.03.012

He, Q, Zhan, H, Shuai, Y, Cai, S, Li, QP, Huang, G and **Li, J.** 2017. Phytoplankton bloom triggered by an anticyclonic eddy: The combined effect of eddy-Ekman pumping and winter mixing. *Journal of Geophysical Research: Oceans*, 122(6): 4886–4901. DOI: https://doi.org/10.1002/2017JC012763

Jing, F, Chauhan, A, Singh, RP and **Dash, P.** 2020. Changes in Atmospheric, Meteorological, and Ocean Parameters Associated with the 12 January 2020 Taal Volcanic Eruption. *Remote Sensing*, 12(6). DOI: https://doi.org/10.3390/rs12061026

Kubryakov, AA, Zatsepin, AG and **Stanichny, SV.** 2019. Anomalous summer-autumn phytoplankton bloom in 2015 in the Black Sea caused by several strong wind events. *Journal of Marine Systems*, 194: 11–24. DOI: https://doi.org/10.1016/j.jmarsys.2019.02.004

Kundu, SN, Sahoo, AK, Mohapatra, S and **Singh, RP.** 2010. Change analysis using IRS-P4 OCM data after the Orissa super cyclone. *International Journal of Remote Sensing*, 22(7): 1383–1389. DOI: https://doi.org/10.1080/01431160119932

Kuttippurath, J, Sunanda, N, Martin, MV and **Chakraborty, K.** 2021. Tropical storms trigger phytoplankton blooms in the deserts of north Indian Ocean. *npj Climate and Atmospheric Science*, 4(1). DOI: https://doi.org/10.1038/s41612-021-00166-x

Lin, II, Chen, CH, Pun, IF, Liu, WT and **Wu, CC.** 2009. Warm ocean anomaly, air sea fluxes, and the rapid intensification of tropical cyclone Nargis (2008). *Geophysical Research Letters*, 36(3): n/a–n/a. DOI: https://doi.org/10.1029/2008GL035815

Lin, I, Liu, WT, Wu, CC, Wong, GTF, Hu, C, Chen, Z, Liang, WD, Yang, Y and **Liu, KK.** 2003. New evidence for enhanced ocean primary production triggered by tropical cyclone. *Geophysical Research Letters*, 30(13). DOI: https://doi.org/10.1029/2003GL017141

Lü, H, Liu, Y, Chen, X, Zha, G and **Cai, S.** 2021. Effects of westward shoaling pycnocline on characteristics and energetics of internal solitary wave in the Luzon Strait by numerical simulations. *Acta Oceanologica Sinica*, 40(5): 20–29. DOI: https://doi.org/10.1007/s13131-021-1808-0

LÜ, H, Xie, J, Xu, J, Chen, Z, Liu, T and **Cai, S.** 2016. Force and torque exerted by internal solitary waves in background parabolic current on cylindrical tendon leg by numerical simulation. *Ocean Engineering*, 114: 250–258. DOI: https://doi.org/10.1016/j.oceaneng.2016.01.028

MacKinnon, JA and **Gregg, MC.** 2003. Mixing on the Late-Summer New England Shelf—Solibores, Shear, and Stratification. *Journal of Physical Oceanography*, 33(7): 1476–1492. DOI: https://doi.org/10.1175/1520-0485(2003)033<1476:MOTLNE>2.0.CO;2

Neetu, S, Lengaigne, M, Vincent, EM, Vialard, J, Madec, G, Samson, G, Ramesh Kumar, MR and **Durand, F.** 2012. Influence of upper-ocean stratification on tropical cyclone-induced surface cooling in the Bay of Bengal. *Journal of Geophysical Research: Oceans*, 117(C12): n/a–n/a. DOI: https://doi.org/10.1029/2012JC008433

Osborn, TR. 1980. Estimates of the Local Rate of Vertical Diffusion from Dissipation Measurements. *Journal of*

Physical Oceanography, 10(1): 83–89. DOI: https://doi.org/10.1175/1520-0485(1980)010<0083:EOTLRO>2.0.CO;2

Qiu, G, Xing, X, Chai, F, Yan, XH, Liu, Z and **Wang, H.** 2021. Far-Field Impacts of a Super Typhoon on Upper Ocean Phytoplankton Dynamics. *Frontiers in Marine Science*, 8. DOI: https://doi.org/10.3389/fmars.2021.643608

Qiu, Z, Jiao, M, Jiang, T and **Zhou, L.** 2020. Dam Structure Deformation Monitoring by GB-InSAR Approach. *IEEE Access*, 8: 123287–123296. DOI: https://doi.org/10.1109/ACCESS.2020.3005343

Sarangi, RK, Mishra, MK and **Chauhan, P.** 2015. Remote Sensing Observations on Impact of Phailin Cyclone on Phytoplankton Distribution in Northern Bay of Bengal. *IEEE Journal of Selected Topics in Applied Earth Observations and Remote Sensing*, 8(2): 539–549. DOI: https://doi.org/10.1109/JSTARS.2014.2347036

Singh, RP, Dey, S, Bhoi, S, Sun, D, Cervone, G and **Kafatos, M.** 2006. Anomalous increase of chlorophyll concentrations associated with earthquakes. *Advances in Space Research*, 37(4): 671–680. DOI: https://doi.org/10.1016/j.asr.2005.07.053

Sprintall, J and **Tomczak, M.** 1992. Evidence of the barrier layer in the surface layer of the tropics. *Journal of Geophysical Research*, 97(C5). DOI: https://doi.org/10.1029/92JC00407

Subrahmanyam, B, Rao, KH, Srinivasa Rao, N, Murty, VSN and **Sharp, RJ.** 2002. Influence of a tropical cyclone on Chlorophyll-a Concentration in the Arabian Sea. *Geophysical Research Letters*, 29(22): 22-21-22-24. DOI: https://doi.org/10.1029/2002GL015892

Sun, P, Zhang, K, Wu, S, Wang, R and **Wan, M.** 2021. An investigation into real-time GPS/GLONASS single-frequency precise point positioning and its atmospheric mitigation strategies. *Measurement Science and Technology*, 32(11): 115018. DOI: https://doi.org/10.1088/1361-6501/ac0a0e

Tan, S, Shi, J, Wang, G, Xing, X and **Lü, H.** 2022. A case study of the westward transport of Chorophyll-a entrained by ocean eddies during a tropical cyclone. *Regional Studies in Marine Science*, 52. DOI: https://doi.org/10.1016/j.rsma.2022.102256

Tang, D, Zhao, H, Satyanarayana, B, Zheng, G, Singh, RP, Lv, J and **Yan, Z.** 2009. Variations of chlorophyll-a in the northeastern Indian Ocean after the 2004 South Asian tsunami. *International Journal of Remote Sensing*, 30(17): 4553–4565. DOI: https://doi.org/10.1080/01431160802603778

Vinayachandran, PN. 2003. Phytoplankton bloom in the Bay of Bengal during the northeast monsoon and its intensification by cyclones. *Geophysical Research Letters*, 30(11). DOI: https://doi.org/10.1029/2002GL016717

Wang, T, Zhang, S, Chen, F, Ma, Y, Jiang, C and **Yu, J.** 2020. Influence of sequential tropical cyclones on phytoplankton blooms in the northwestern South China Sea. *Journal of Oceanology and Limnology*, 39(1): 14–25. DOI: https://doi.org/10.1007/s00343-020-9266-7

Wang, W, Shi, K, Zhang, Y, Li., N, Sun, X, Zhang, D, Zhang, Y, Qin, B and **Zhu, G.** 2022. A ground-based remote sensing system for high-frequency and real-time monitoring of phytoplankton blooms, 439: 129623. DOI: https://doi.org/10.1016/j.jhazmat.2022.129623

Zhao, H, Han, G, Zhang, S and **Wang, D.** 2013. Two phytoplankton blooms near Luzon Strait generated by lingering Typhoon Parma. *Journal of Geophysical Research: Biogeosciences*, 118(2): 412–421. DOI: https://doi.org/10.1002/jgrg.20041

Zhao, H, Shao, J, Han, G, Yang, D and **Lv, J.** 2015. Influence of Typhoon Matsa on Phytoplankton Chlorophyll-a off East China. *PLoS One*, 10(9): e0137863. DOI: https://doi.org/10.1371/journal.pone.0137863

Zhao, H, Tang, D and **Wang, D.** 2009. Phytoplankton blooms near the Pearl River Estuary induced by Typhoon Nuri. *Journal of Geophysical Research*, 114(C12). DOI: https://doi.org/10.1029/2009JC005384

Zhou, L, Tian, J and **Wang, D.** 2005. Energy distributions of the large-scale horizontal currents caused by wind in the baroclinic ocean. *Science in China Series D: Earth Sciences*, 48(12): 2267–2275. DOI: https://doi.org/10.1360/04yd0125

TO CITE THIS ARTICLE:
Zhou, Y, LÜ, H, Huang, H, Bai, L, Ding, X, Chen, Z. 2024. A Case Study on Phytoplankton Blooms Triggered by Tropical Cyclone Emeraude in the Central Indian Ocean. *Tellus A: Dynamic Meteorology and Oceanography*,76(1): 101–114. DOI: https://doi.org/10.16993/tellusa.3242

Submitted: 08 June 2023 **Accepted:** 22 April 2024 **Published:** 14 May 2024